Eur. Phys. J. D **16**, 317–320 (2001)

THE EUROPEAN PHYSICAL JOURNAL D

EDP Sciences

Formation and manipulation of regular metallic nanoparticle arrays on bacterial surface layers: an advanced TEM study

M. Mertig[1,a], R. Wahl[1], M. Lehmann[2], P. Simon[2], and W. Pompe[1,b]

[1] Institut für Werkstoffwissenschaft, Technische Universität Dresden, D-01069 Dresden, Germany
[2] Institut für Angewandte Physik (IAPD), Technische Universität Dresden, D-01069 Dresden, Germany

Received 6 December 2000

Abstract. The template-directed formation of regular nanoparticle arrays on two-dimensional crystalline protein layers after their treatment with metal salt complexes was studied by transmission electron microscopy. For these investigations, bacterial surface layers (S layers), recrystallized *in vitro* into sheets and tube-shaped protein crystals with typical dimensions in the micrometer range, were used as the template. As identified by electron holography and scanning force microscopy, the S-layer tubes form alternating double layers when deposited onto a solid substrate surface. Two distinct pathways for the metal particle formation at the templates have been found: the site-specific growth of metal clusters by chemical reduction of the metal salt complexes, and the electron-beam induced growth of nanoparticles in the transmission electron microscope. Both mechanisms lead to regular arrays with particle densities $> 6 \times 10^{11}$ cm^{-2}. Nanoparticle formation by electron exposure takes exclusively place in the flat-lying double-layered protein tubes, where a sufficient amount of metal complexes can be accumulated during sample preparation.

PACS. 82.30.Nr Association, addition, insertion, cluster formation – 68.37.Lp Transmission electron microscopy (TEM) (including STEM, HRTEM, etc.) – 82.35.Pq Biopolymers, biopolymerization

1 Introduction

With progressive miniaturisation of electronic and optical devices there is an increasing interest in the development of advanced methods for the bottom-up construction of functional nanostructures. In particular, the use of biological molecules and structures constitutes a very promising approach for the organisation of inorganic materials at the nanometer length scale [1]. Due to the well defined chemical, physical and structural properties of the templates, the method of biomolecular templating allows parallel fabrication of desired inorganic nanostructures of different morphology [2–7]. Especially, regular S layers are found to be well suited as templates for the predefined fabrication of ordered metallic and semiconducting cluster arrays [8–10]. S layers are regular quasi two-dimensional protein crystals with a thickness of 5 to 15 nm. They constitute the outermost component of the cell envelope of many bacteria and archaea [11–13], exhibit different lattice symmetries with lattice constants ranging from 3 to 30 nm and possess nanopores of well-defined size. S layers are composed of periodically-arranged identical subunits leading to a precise spatial arrangement of physicochemical affinity sites at the protein surface, that can be used to accomplish a site-specific chemistry. These particular properties allow to employ S layers for the template-directed parallel fabrication and manipulation of metal clusters with a narrow size distribution [10]. Moreover, the possibility to reconstitute S layers *in vitro* into large-area two-dimensional crystals [14] makes them an almost ideal biomolecular template for supramolecular engineering.

Here, we report two different methods of the formation of regular cluster arrays on the S layer of *Bacillus sphaericus* NCTC 9602: the chemical deposition of metallic clusters, and the template-directed synthesis of Pt and Pd nanoparticle arrays in the transmission electron microscope. In the latter method, the simultaneous growth of ordered nanoparticles is solely initiated by electron exposure. That is, the metal clusters are manipulated in parallel. Furthermore, advanced transmission electron microscopy (TEM) methods like electron holography [15] are exploited for the sample characterisation.

2 Experimental

The S-layer protein was isolated from *Bacillus sphaericus* NCTC 9602 cells. The cell cultivation conditions and protein purification are described elsewhere [16,17]. The obtained S-layer preparation was washed, resuspended in

[a] e-mail: mertig@tmfs.mpgfk.tu-dresden.de

[b] The authors wish to thank S. Selenska-Pobell and J. Raff for stimulating discussions concerning the interaction of transition metals with proteins and for purification of the protein, and H. Lichte for a critical reading of the manuscript.

a phosphate buffer solution (50 mM KH_2PO_4/Na_2HPO_4, pH 7.5, 1 mM $MgCl_2$, 3 mM NaN_3) and stored at 4 °C. For the large scale recrystallization of the protein template, first the S-layer preparation was centrifuged at 20.000 g for 60 min at 4 °C. Then the pellet was solved in about ten times the amount of guanidine hydrochloride (7.5 M in 50 mM TRIS hydrochloride buffer, pH 7.4) to disintegrate the native S-layer sheets into protein monomers. Thereafter, the sample was dialysed against 10 mM $CaCl_2$ for more than 2 hours at 4 °C. During this time the monomers reassembled in the form of larger S-layer sheets and tubes. The assembly products were again centrifuged and resuspended in phosphate buffer.

To activate the recrystallized S-layer structures, 20 μl of S-layer suspension containing $\approx$ 10 mg/ml protein were treated with 1 ml of hydrolysed 3 mM K_2PtCl_4 or K_2PdCl_4 solution at room temperature. The incubation time of S layers was varied between a few minutes up to 30 h.

The TEM and scanning force microscopy (SFM) samples were prepared by placing a droplet of activated S-layer suspension onto a TEM grid for about 1 min and then removing excess solution with a filter paper. After this, the samples were air-dried. Carbon-coated finder grids with letter markers were used to allow direct comparison of special features in TEM and SFM. For the structure investigations on non-activated S layers the preparations were negatively stained with 2% uranyl acetate.

TEM investigations as well as off-axis electron holography have been performed at a 200 kV Philips CM200-FEG electron microscope equipped with a Lorentz lens. The electron holograms are recorded by means of a Moellenstedt biprism which superimposes an unmodulated reference wave to the object-modulated electron wave yielding an interference pattern, the so-called electron hologram. The reconstruction of the hologram using the laws of Fourier optics yields two separate images, the amplitude and the phase image. The phase image mainly represents the wave optical path difference of the modulated and unmodulated electron waves. In the domain of nm-scale the phase is proportional to the mean inner potential multiplied to the specimen thickness. Therefore, electron holography can be used to determine the relative thickness of the sample. The holograms were recorded in slight underfocus with the objective lens switched-off and the Lorentz lens switched-on, since this electron optical setup provides larger field of views of 500 nm and higher. The SFM investigations were carried out with a Digital Instruments NanoScope IIIa in tapping mode.

3 Results and discussion

The recrystallized S-layer sheets of *B. sphaericus* NCTC 9602 exhibit a square lattice symmetry with a lattice constant of 12.5 ± 0.8 nm (Fig. 1). The image reconstruction by FFT filtering shows that the protein units are slightly tilted with respect to the major symmetry axes of the lattice.

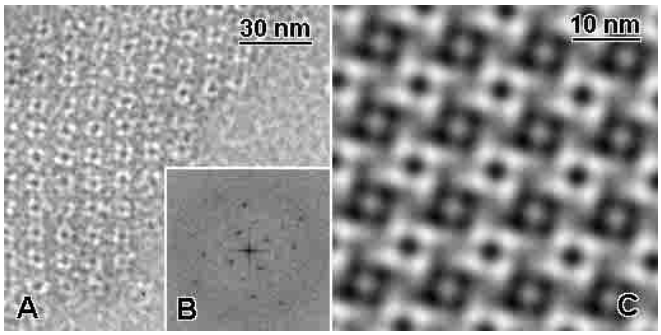

Fig. 1. S-layer of *B. sphaericus* NCTC 9602: A - TEM micrograph of the negatively stained S layer, B - power spectrum of A, C - reconstructed S-layer lattice obtained by noise filtering of B.

Besides S-layer sheets, the recrystallization in bulk solution resulted in the formation of open-ended S-layer tubes with a length up to 10 μm and diameters ≤ 1 μm. As revealed by SFM, the adsorption of such tubes on the TEM grids led to flat-lying double-layered band-shaped protein structures at which the larger corrugated cytoplasmic surface of the S layer [12] is located inside the tubes (not shown). When deposited to the substrate, the tubes fold solely along the [11]–direction of the protein crystal. Therefore, the larger corrugations come into register and form small cavities located between the alternatively oriented layers of the tube. One cavity per unit cell with a lateral size of about 6 nm is formed. We have applied electron holography to identify double-layered protein tubes by measuring the relative thickness of these protein assemblies. The double layers were analysed in the reconstructed phase image since the phase shift doubles with respect to a single layer (Fig. 2). The ends of the tubes are mostly frayed-out; hence one finds at this part of the specimen both mono and double layered areas. Since the unstained samples exhibited electrical charging which falsified the information in the reconstructed phase, the holographic investigations were only performed at stained specimen. Up to now, the holograms were recorded with broad interference fringes, leading to a limited spatial resolution of the reconstructed images. Therefore, the lattice structure is not resolved in the reconstructed amplitude and phase. However, the spatial resolution can still be improved down to the given information limit of the Lorentz lens (1.3 nm), which is part of our future activities.

The long-time treatment ($>$ 5 h) of the S-layer suspensions with hydrolysed Pt or Pd complexes leads to the formation of ordered metal cluster arrays at the template (Fig. 3A). These clusters, nucleated at the biomolecular template, are formed by chemical reduction of metal salt complexes. Here, the used phosphate buffer itself, which contains small amounts of NaN_3, acts as very mild reduction agent.

The well separated clusters have a diameter of 2 to 3 nm. Fig. 3C reveals that the lateral cluster arrangement is completely determined by the p4 symmetry of the underlying protein lattice. This result is in agreement with previous experiments, where regular cluster arrays were

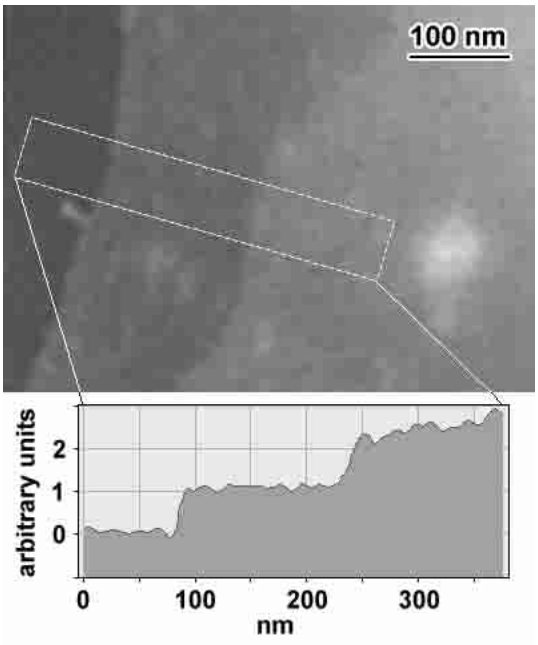

Fig. 2. Height analysis of one open end of a self-assembled negatively stained S-layer tube. Upper image - reconstructed phase of an electron hologram. Lower image - corresponding profile. A stepwise transition from a mono- to a double-layered protein structure is observed.

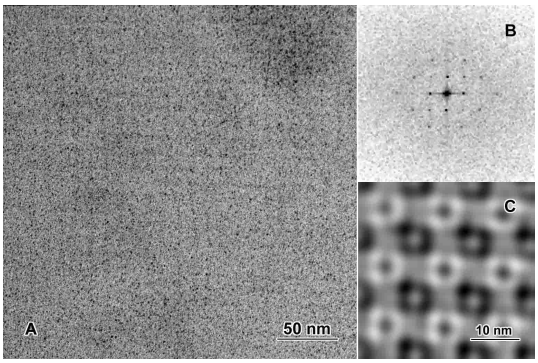

Fig. 3. Platinum clusters chemically deposited onto the S layer of *B. sphaericus* NCTC 9602: A - TEM micrograph, B - Fourier spectrum of A, C - image reconstruction after filtering of B.

fabricated on the S layer of *Sporosarcina ureae* [10]. The observed particle pattern is nearly identical to that of the negatively-stained protein crystal (*cf.* Fig. 1C). This implies that the cluster formation takes place at the same positions where the stain is accumulated, *i.e.* in the pores of the S layers. However, contrary to the staining with uranyl acetate, the formed Pt or Pd clusters appear well separated. They are still bound after repeated washing of the sample. The preferential growth of clusters in the pores of the S-layer template clearly indicates that the pores are distinguished sites for the heterogeneous nucleation of clusters. Site-specific nucleation will take place when the concentration of metal complexes adsorbed in the pores gets high enough to become critical for cluster nucleation. Thus, the presented results unambiguously show that the pores of S layers constitute specific affinity sites for the metal deposition. However, the reason for the enhanced affinity in the pores is not yet understood.

The metallic character of the clusters grown on S-layers was confirmed by high-resolution TEM (HRTEM) investigations. Fig. 4 shows an example for Pt clusters, where the lattice spacings are determined as 0.22 nm and 0.19 nm identifying the (111) and (202) planes, respectively, of a pure metallic Pt phase with an unit cell size of about 0.39 nm.

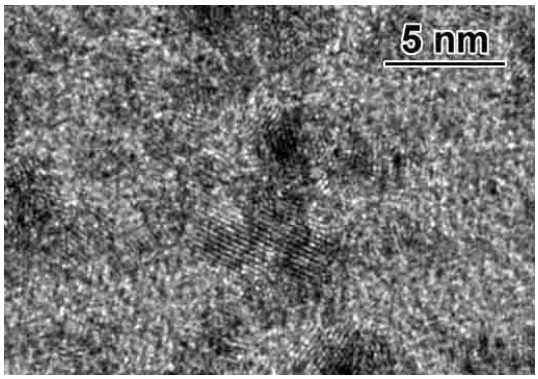

Fig. 4. HRTEM micrograph of a Pt-cluster array on the S layer of *B. sphaericus* NCTC 9602.

A completely different result is obtained for short-time activation. Treatment times of a few minutes up to 2 hours are not sufficient for nucleation and growth of metal clusters to occur by chemical deposition. However, we observe a different mechanism of metal particle formation, caused by electron exposure in the transmission microscope [17]. Electron-beam induced reduction to the metallic state in an electron microscope was first reported for tungsten trioxide [18] and Pd acetat [19]. In our case, however, this mechanism leads to the formation of periodically arranged nanoparticle arrays because of the specific geometry of the used S-layer templates (Fig. 5). The metallic character of the nanoparticles was confirmed by HRTEM investigations (not shown).

For the electron-beam induced growth of nanometer-sized metal particles, it is necessary to accumulate the metal complexes at sufficiently high concentrations on the specimen prior to electron exposure. This requirement can be met in a particular way during the deposition of tube-shaped S-layer assemblies onto the substrate surface. When tubes, still filled with metal salt solution, are deposited onto a rapidly drying substrate surface, we observe that an appreciable amount of metal complexes is accumulated between the inner, cytoplasmic surfaces of the tubes [17]. Localized patches with a sufficiently high complex concentration are formed, not covering the complete sectional area of the flat-lying band-shaped tubes. Only in that area nanoparticles start to grow within the time of a few minutes when the samples are exposed to the electron beam, explaining why the nanoparticle arrays exhibit a non-regular shape as seen in Fig. 5. Interestingly, the shape of the growing particles, their

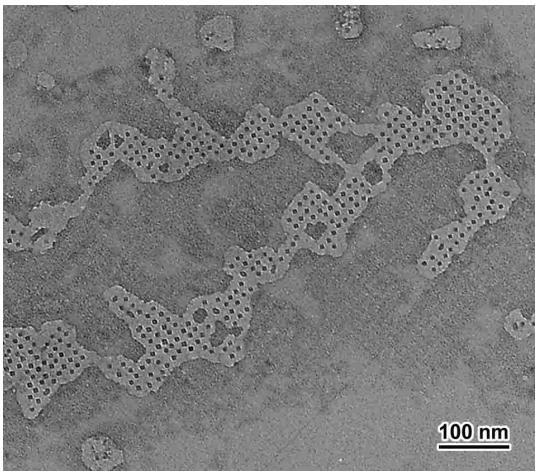

Fig. 5. TEM micrograph of highly-ordered platinum particles formed by electron-beam induced nucleation in a recrystallised S-layer tube of *B. sphaericus* NCTC 9602 after 80 min of treatment with K_2PtCl_4.

interparticle distances and the symmetry of the particles are entirely determined by the S-layer template. The particle exhibit a square-like shape with a lateral size of 5 to 7 nm. The squares are slightly tilted with respect to the major symmetry axes of the array. The particle arrays show a fourfold symmetry with a periodicity which corresponds to the lattice constant of the protein crystal. Therefore, we conclude that the nanoparticles grow preferentially in the small cavities between the inner, cytoplasmic surfaces of the flat-laying tubes. In distinction to that, electron-beam induced nanoparticle formation was not observed at monolayers, since metal salt trapping does not occur at S-layer sheets. The nucleation of Au clusters on recrystallized monolayers of the S layer of *B. sphaericus* CCM 2177 in the TEM due to the thermal effect of the radiation was reported in an alternative approach by Dieluweit *et al.* [9]. In their experiment the Au complexes are bound to the protein surface prior to the electron exposure by chemical modification of the S layer with thiol groups. In our investigations the Pt and Pd complexes are physically accumulated due to the particular molecular geometry of recrystallized S-layer tubes.

After long-time exposure we observed that the nanoparticles start to migrate and finally to agglomerate. Under the assumption that the particle migration is caused by irradiation damage of the supporting protein matrix, our investigations allow to estimate the electron doses relevant for structural protein damage. The nanoparticle formation was accomplished within about 3 min at a dose rate of about $7 \times 10^3 e\ \mathrm{nm}^{-2}\,\mathrm{s}^{-1}$. Within this time approximately 1.8×10^8 electrons pass through each unit cell of the protein lattice which consists of 4 protein monomers of about 130 kDa [20]. This corresponds to a minimum electron dose of about $1.2 \times 10^6 e\ \mathrm{nm}^{-2}$. This value is 10^4 times higher than that reported by Knapek [21] for the damage of biological specimens. We suppose that the difference can be explained by the assumption of stabilisation of the protein structure by the intercalated metal complexes.

4 Summary

The presented results show that periodic nanoparticle arrays can be formed in various ways by a growth of metallic clusters on S layers of *B. sphaericus* NCTC 9602 activated with metal salt complexes. Depending on the particular morphology of the recrystallized protein templates, cluster nucleation can be accomplished chemically or by electron exposure in the transmission electron microscope. In both cases the geometrical properties of the particle arrays are completely determined by the underlying protein templates. Thus, biomolecular templating allows to fabricate and to manipulate metal clusters in parallel.

References

1. S. Mann, *Biomimetic Materials Chemistry* (VCH, New York, 1996).
2. K. Douglas, N.A. Clark, K.J. Rothshild, Appl. Phys. Lett. **48**, 676 (1986).
3. M. Pazirandeh, S. Baral, J.R. Campbell, Biomimetics **1**, 41 (1992).
4. K.K.W. Wong, S. Mann, Adv. Mater. **8**, 928 (1996).
5. R. Kirsch, M. Mertig, W. Pompe, R. Wahl, G. Sadowski, K.J. Böhm, E. Unger, Thin Solid Films, **305**, 248 (1997); M. Mertig, R. Kirsch, W. Pompe, Appl. Phys. A **66**, 723 (1998).
6. J. Richter, R. Seidel, R. Kirsch, M. Mertig, W. Pompe, J. Plaschke, H.K. Schackert, Adv. Mater. **12**, 507 (2000).
7. J. Richter, M. Mertig, W. Pompe, I. Mönch, H.K. Schackert, Appl. Phys. Lett. **78**, 536 (2001).
8. W. Shenton, D. Pum, U.B. Sleytr, S. Mann, Nature **389**, 585 (1997).
9. S. Dieluweit, D. Pum, U.B. Sleytr, Supramol. Sci. **5**, 15 (1998).
10. M. Mertig, R. Kirsch, W. Pompe, H. Engelhardt, Eur. Phys. J. D **9**, 45 (1999).
11. U.B. Sleytr, P. Messner, Ann. Rev. Microbiol. **37**, 311 (1983).
12. U.B. Sleytr, P. Messner, D. Pum, M. Sara, *Crystalline bacterial cell surface proteins* (Academic Press, San Diego, 1996).
13. H. Engelhardt, J. Peters, J. Struct. Biol. **124**, 276 (1998).
14. D. Pum, U.B. Sleytr, Thin Solid Films **244**, 882 (1994).
15. H. Lichte, *Handbook of Microscopy* (VCH, Weinheim, 1997), Vol. 1, p. 515.
16. H. Engelhardt, W.O. Saxton, W. Baumeister, J. Bacteriology **168**, 309 (1986).
17. R. Wahl, M. Mertig, J. Raff, S. Selenska-Pobell, W. Pompe, Adv. Mater. **13**, 736 (2001).
18. J. Singh, L.D. Marks, Philos. Mag. Lett. **60**, 31 (1989).
19. T.J. Stark, T.M. Mayer, D.P. Griffis, P.E. Russell, J. Vac. Sci. Technol. B **9**, 3475 (1991); T.J. Stark, T.M. Mayer, D.P. Griffis, P.E. Russell, J. Vac. Sci. Technol. B **10**, 2685 (1992).
20. A.T. Hastie, C.C. Brinton Jr, J. Bacteriology **138**, 999 (1979).
21. E. Knapek, Ultramicroscopy **10**, 71 (1982).